

XMM-NEWTON STUDIES OF THE SOURCE POPULATION AND THE HOT INTERSTELLAR MEDIUM IN NEARBY GALAXIES

W. Pietsch

Max-Planck-Institut für extraterrestrische Physik, Postfach 1312, 85741 Garching, Germany

ABSTRACT

First results of X-ray source population studies in nearby galaxies show the potential of XMM-Newton observations. I will report on first XMM-Newton M31 results and on three of our XMM-Newton projects, an X-ray source population study in the Magellanic Clouds (MCs), a deep raster survey of M33, and an investigation of the hot interstellar medium (ISM) in the halo of edge-on galaxies. XMM-Newton results on several other galaxies and sources within are presented by other authors in these proceedings.

Our MC study is build up of deep pointings probing MC sources down to 10^{33} erg s⁻¹ and shallower pointings to confirm candidates from our ROSAT derived lists of X-ray binaries (XRBs), super-soft sources (SSSs), and supernova remnants (SNRs). First XMM-Newton detections of a 455 s pulsar in the Small Magellanic Cloud (SMC) and the results of the Large Magellanic Cloud (LMC) deep field confirm the validity of our strategy.

Our M33 raster pointing aims for luminosities as low as 10^{35} erg s⁻¹, a factor of 10 below the sensitivity limit of the ROSAT observations. The survey will allow us to characterize the sources using extent, spectra, hardness ratios and time variability to build up a unprecedented census of the X-ray source content of M33. Of specific interest are the active source in the nuclear area and the diffuse emission in the inner disk.

XMM-Newton observations of the active galaxy NGC 3079 and of the starburst galaxy NGC 253 are used to characterize the point-like sources and the hot ISM in the disk and from the halo of these galaxies.

Key words: X-rays: galaxies – galaxies: spiral – galaxies: ISM

an active nucleus (AGN) could be detected (sometimes heavily absorbed) dominating the galaxy's X-ray emission. The imaging proportional counters aboard *Einstein* (IPC) and ROSAT (PSPC) were able to spatially resolve these components. However, the energy resolution was only sparse. The CCD detectors aboard the ASCA and BeppoSAX observatories on the other hand provided much better energy resolution and a broader energy coverage. However with the poorer spatial resolution, in most cases it was not possible to resolve the different emission components. The average parameters extracted for the galaxies as a whole, are of rather limited value.

With the new generation X-ray observatories *Chandra* and XMM-Newton, we now have the sensitivity and spatial and spectral resolution to probe significantly deeper. The high throughput of XMM-Newton combined with the spatial resolution comparable to the ROSAT high resolution imager (HRI) allows us in X-ray source population studies (1) to detect sources more than a factor of 10 deeper than before; (2) to classify the sources in a broad X-ray energy band (spectra, hardness ratios, variability, extent, pulsations); (3) to determine log N / log S distributions. For the hot ISM, we are able (1) to resolve it from X-ray point sources; (2) to analyze the spatial variability of its X-ray spectrum with medium and high energy resolution. With the results for different galaxies, we can search for dependencies of the X-ray parameters on galaxy type, metallicity, and star forming history.

In the following I will report on XMM-Newton results that demonstrate these possibilities. Interesting additional new XMM-Newton results on M31, NGC 300 and other nearby galaxies (and individual sources within) will be presented in these proceedings.

2. FIRST RESULTS ON M31

The Andromeda Galaxy (M31) is the closest big spiral galaxy to our own and was observed as a XMM-Newton performance verification (PV) target in order to demonstrate the capabilities of the mission in performing spectral and timing studies in a field of point sources and extended emission.

In a first paper Shirey et al. (2001) focused on the group properties of the X-ray point sources and on the diffuse emission. They detect 116 sources in the central 30' of M31 down to a limiting luminosity of 6×10^{35} erg s⁻¹.

1. INTRODUCTION

Observations of the *Einstein* and ROSAT observatories demonstrated that the X-ray emission of nearby late type galaxies (spirals and irregulars) can be separated in contributions from point-like sources (low- and high-mass XRBs, SSS, young supernovae, SNRs, etc.) and diffuse emission (hot ISM within the disk, from an outflow, or from the galaxy halo). In some of the galaxies X-ray emission from

The luminosity distribution of the sources flattens at luminosities below $\sim 2.5 \times 10^{37}$ erg s $^{-1}$. The detected sources can be classified into source classes such as SSSs and intrinsically hard or soft sources using hardness ratios. The spectrum of the unresolved emission in the bulge of M31 is demonstrated to contain a soft excess. It can be fitted with a 0.35 keV optically-thin thermal-plasma component from diffuse hot gas in the center of M31 which is clearly distinct from the composite point-source spectrum. The extended emission can clearly be seen in the image.

In a second paper Osborne et al. (2001) discussed the variability of individual sources in M31 based on PV observations in June and December 2000. For the ~ 60 brightest sources they searched for time variability. At least 15% of the sources appear to be variable on a time scale of several months. A bright new transient source detected close to the nucleus in June, was no longer detectable in the December observation and may be similar to some Galactic low mass XRBs, most of which are supposed to harbour black holes. They also detected a 865 s period from a SSS, which was significantly fainter in the second observation. This source may be a rapidly spinning magnetized white dwarf in a symbiotic nova system.

3. MAGELLANIC CLOUD STUDIES

The ‘first light’ target of XMM-Newton was the X-ray rich LMC region close to 30 Doradus and supernova SN1987A (Dennerl et al. 2001). The X-ray spectrum of several SNRs in the field was analyzed using the EPIC cameras. The hot ISM in the area indicates significant overabundance of Ne and Mg. Column densities derived from the EPIC spectra of several AGN shining through the interstellar gas of the LMC compared with HI measurements, will allow to draw conclusions on LMC atomic to molecular hydrogen ratios (Haberl et al. 2001).

Several more LMC and SMC sources were observed as calibration and PV targets and characterized by high resolution RGS or EPIC spectra. Examples are the SNRs 1E 0102.2-7219 (Rasmussen et al. 2001, Sasaki et al. 2001a), N132D (Behar et al. 2001), SNR B0540-69.3 (van der Heyden et al. 2001), and the SSS CAL 83 (Paerels et al. 2001). For the candidate black hole XRB LMC X-3, EPIC and RGS observations cover the soft and hard spectral state (Wu et al. 2001). OM filter observations let to a more accurate lower mass limit of the compact object in LMC X-3 (Soria et al. 2001).

We analyzed in detail of all ROSAT PSPC and HRI observations of the MC which led to large catalogues of X-ray sources (LMC: Haberl & Pietsch 1999, Sasaki et al. 2000a; SMC: Haberl et al. 2000, Sasaki et al. 2000b) which we characterized by their hardness ratios and extent and partly identified by cross-correlations with catalogues at other wavelengths. To follow up on this work, we proposed deep field observations in some areas and shallower obser-

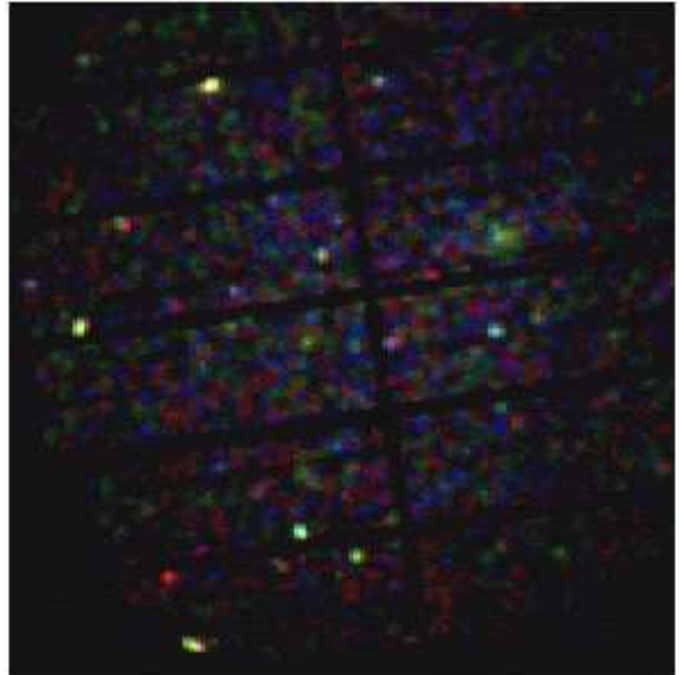


Figure 1. EPIC PN image of a $\sim 13'$ radius region around SMC X-2. The colours represent X-ray intensities in different energy bands (red: 0.2–1.0 keV, green: 1.0–2.0 keV, blue: 2.0–5 keV). Red objects are foreground stars. The other objects are high mass XRB candidates or background active nuclei. The transient pulsar SMC X-2 was detected in quiescence (blue object in the center). The extended greenish object in the NW is most likely a new SMC SNR.

vations of some XRB and SNR candidates to search for periods and/or measure extent and spectra.

Haberl (see these proceedings) reports on an LMC deep guaranteed time (GT) pointing to a field containing three high mass XRBs which were identified in ROSAT studies during outburst. The XRBs are detected with the XMM-Newton EPIC instruments in quiescence and still periods can be derived. In a preliminary overall analysis of the field, about 150 X-ray sources are detected down to fluxes of 10^{-14} erg cm $^{-2}$ s $^{-1}$, while ROSAT only detected 35 sources in the field. New faint SNRs and XRBs are detected and also a class of new faint sources that most likely represent low mass XRBs and/or cataclysmic variables in the LMC and are not background AGN.

During October 2001, a series of XMM-Newton pointings was started to further constrain our list of ROSAT SMC XRB candidates and detect new XRBs and XRB pulsars in the SMC. The first target was the area around the Be/XRB transient SMC X-2 (see Fig. 1). Unfortunately, the observation suffered from high EPIC background. Nevertheless, we did not only detect SMC X-2 in quiescence at a luminosity as low as 1.5×10^{33} erg s $^{-1}$, but besides foreground stars, also a new SNR and high

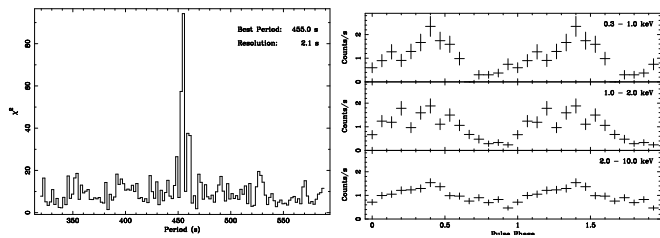


Figure 2. XMM-Newton EPIC PN detection of 455 s pulsation from the Be/XRB RX J0101.3-7211: (Left) χ^2 periodogram, showing the strong signal at the proposed period. (Right) light curve folded modulo 455 s for 3 energy bands.

mass XRB candidates (from comparison with digital sky survey images).

We also tried to use calibration and PV observations to prove our search strategy for XRB pulsars. We serendipitously detected the ROSAT Be/XRB candidate RX J0101.3-7211 in the EPIC PN instrument at the outer boarder of a SNR 0102-72.3 observation (Sasaki et al. 2001b). The luminosity of RX J0101.3-7211 determined during the observation with the XMM-Newton EPIC PN in the ROSAT band (2.5×10^{34} erg s $^{-1}$), was lower than during the faintest ROSAT detection; the X-ray spectrum can be described by a power-law with photon index of 0.6. A timing analysis of the data revealed 455 s pulsations (Fig. 2) that are clearly detectable in the energy bands 0.3–1.0, 1.0–2.0, and 2.0–10.0 keV with a slight shift of the minimum to earlier phases in the softest band. These findings together with optical spectra of the proposed counterpart confirm RX J0101.3-7211 as SMC Be/XRB.

4. XMM-NEWTON M33 RASTER OBSERVATION

Besides M31 and the MCs the Sc spiral M33 seen near face-on, belongs to the galaxies in the Local Group best studied in X-rays. We carefully analyzed all M33 ROSAT observations in the archive and found 184 X-ray sources within 50' of the nucleus. We partly classified and identified the sources by correlations with previous catalogues and using their X-ray properties. M33 is known to harbour a bright active source in the nuclear area, several SSSs, SNRs, and XRB candidates (see Haberl & Pietsch 2001 and references therein). For one of the sources, eclipses with a period of 3.45 d and a possible 0.31 s pulsation period strongly suggest a high mass XRB nature (Dubus et al. 1999).

As a GT program we proposed fifteen 10 ks pointings to homogeneously cover M33 to unprecedented depth (better than 10^{35} erg s $^{-1}$ within the optical D_{25} diameter) and smooth out residual EPIC detector structures by this raster. The first five observations were performed in August 2000 and confirmed our strategy (see Pietsch et al. 2000b and Ehle et al. 2001).

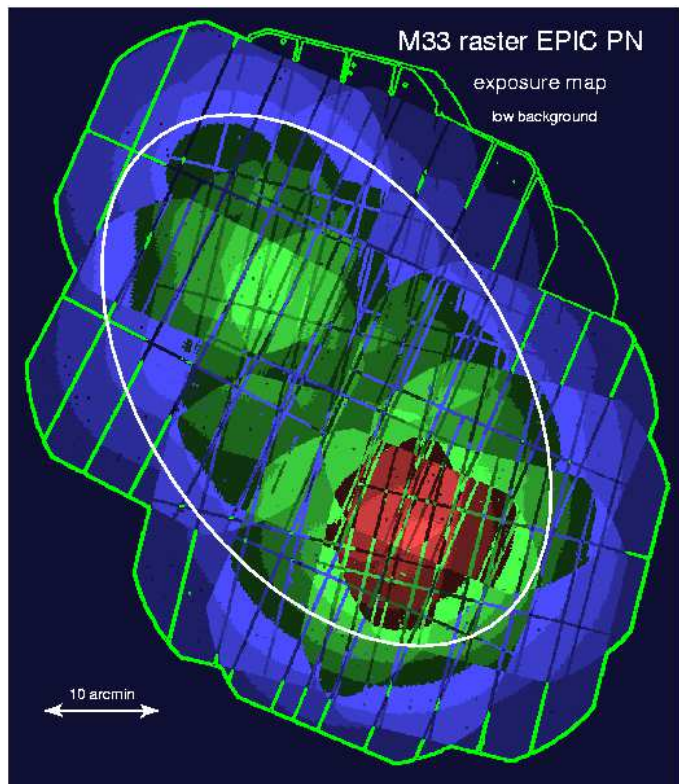


Figure 3. Exposure map of the EPIC PN low background times for the 12 M33 raster observations. Blue colours give exposures from 0–10 ks, green from 10–20 ks and red from 20–30 ks. The white ellipse indicates the optical D_{25} diameter of the galaxy.

Until August 2001, seven more pointings of the raster were performed. Unfortunately, one of the observations was rather short and several others suffer from high detector background. To produce homogeneous images and to reach highest sensitivity for faint sources and diffuse emission from M33, we had to reject high background times. The resulting combined low background EPIC PN exposure map for the 12 raster observations is shown in Fig. 3. While in the SW part of the M33 disk we achieve an exposure of ~ 30 ks, the central and NE part is much less exposed.

Figure 4 gives a slightly smoothed EPIC PN low background image of the M33 raster in the 0.2–7.2 keV band, Fig. 5 the corresponding colour image (red: 0.2–1.0 keV, green: 1.0–2.0 keV, blue: 2.0–7.2 keV). The optical D_{25} diameter is indicated. In Fig. 4, ROSAT sources from Haberl & Pietsch (2001) are superimposed. To create the images we used photon event lists with sky coordinates transformed to a common reference point. For each observation we separately created low background images for the 0.2–0.5, 0.5–1.0, 1.0–2.0, and 2.0–7.2 keV bands and accepted just single events for the lowest energy band, singles and doubles for the other bands. We subtracted ‘out

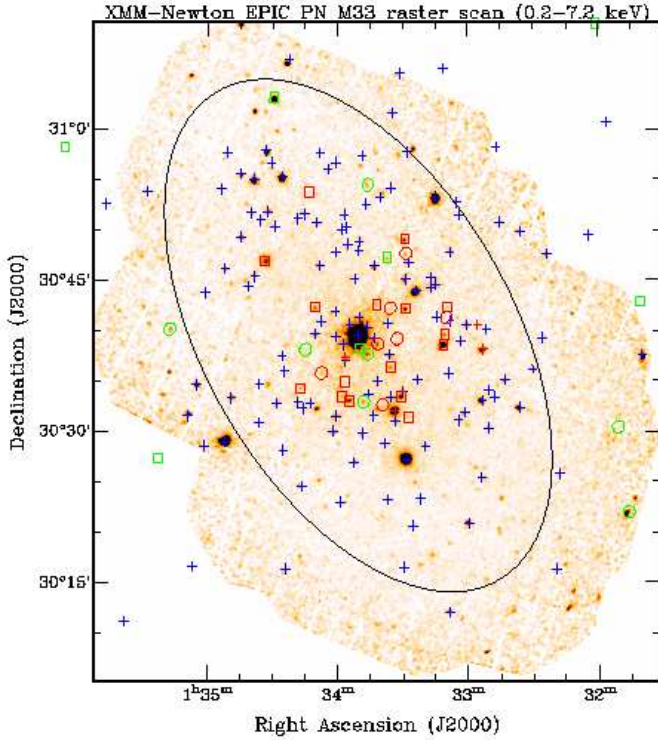


Figure 4. EPIC PN low background image of the 12 M33 raster observations (0.2–7.2 keV). The black ellipse indicates the optical D_{25} diameter of the galaxy. ROSAT sources from Haberl & Pietsch (2001) are superimposed. Classified sources are indicated: SNRs by red squares, SSS by red circles, XRBs by red crosses, foreground stars by green circles, background AGN by green squares. Blue crosses indicate unclassified sources.

of time event’ images. We also created individual exposure maps. The resulting individual images and exposure maps were masked for low exposure and then combined. The combined images were exposure corrected and finally the images for the bands were added as needed.

A large number of point-like sources (several of which were identified by ROSAT before, see Haberl & Pietsch 2001), some diffuse sources and strong emission from the nuclear area are clearly visible. Diffuse emission is detected surrounding the bright nucleus and from the location of the optically bright southern spiral arm. The colour image shows SSS in red, SNRs in yellow, and XRBs as well as background AGN in white or blue. The extended red object NE of the nucleus is the giant H II region NGC 604.

To better characterize the sources, we performed spectral fits to the EPIC PN data of the brightest sources and produced light curves. EPIC MOS data will be added. Some first results are given below.

The nuclear source is the most luminous persistent source in the Local Group (unabsorbed 0.3–10 keV luminosity of $\sim 1.2 \times 10^{39}$ erg s $^{-1}$). Its EPIC PN spectrum can be described by a disk-blackbody plus power

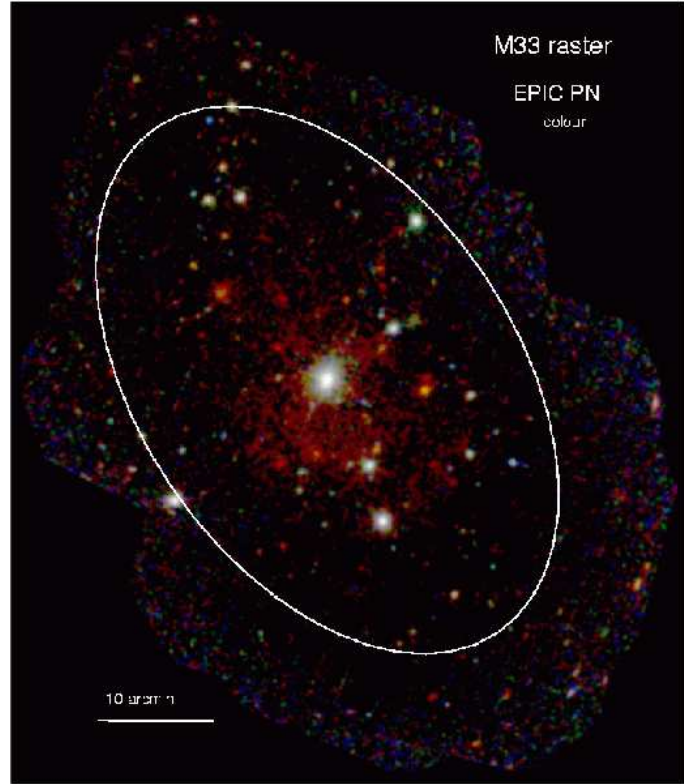


Figure 5. EPIC PN low background image of the 12 M33 raster observations. The colours represent X-ray intensities in different energy bands (red: 0.2–1.0 keV, green: 1.0–2.0 keV, blue: 2.0–7.2 keV). The white ellipse indicates the optical D_{25} diameter of the galaxy.

law model typical for black hole XRBs. The best fit parameters during the pointing when the source was in the center of the field, are: $N_{\text{H}} = 2.1 \times 10^{22}$ cm $^{-2}$, well above the Galactic value, photon index 2.6, temperature $kT_{\text{in}} = 1.2$ keV at the inner disk radius, $R_{\text{in}} \cos(i)^{0.5} = 31$ km, yielding an estimated Schwarzschild black hole mass of $\sim 3.5 \cos(i)^{-0.5} M_{\odot}$. No time variability was detected during this observation. RGS spectra are in good agreement with the EPIC PN results and do not show any significant emission or absorption lines.

Several XRB and SSS candidates show variability within individual observations. The Dubus et al. (1999) high mass XRB was in the field of view during seven pointings. In two observations at extrapolated binary phases 0.0 and 0.1, it was faint, while during the rest of the observations (at phases 0.2 to 0.6), it showed no variability. A background AGN candidate showed an absorbed power law spectrum with a photon index of 2.0.

5. HOT ISM IN EDGE-ON GALAXIES

ROSAT has detected diffuse emission from the hot ISM in the disk, from outflowing winds (e.g. the ‘plume’ in NGC 253 extending more than 1’ to the SE from the nu-

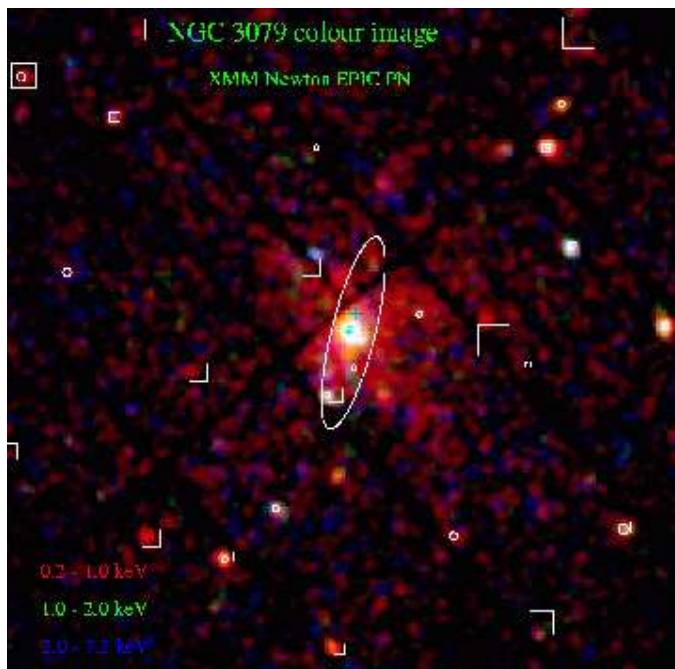


Figure 6. EPIC PN low background image for the NGC 3079 field. The colours represent X-ray intensities in different energy bands (red: 0.2–1.0 keV, green: 1.0–2.0 keV, blue: 2.0–7.2 keV). The white ellipse indicates the optical D_{25} diameter of the galaxy. ROSAT PSPC sources from Pietsch et al. (1998) are indicated by squares, HRI sources by circles. The symbol size represents the 90% confidence positional error. The position of SN 2001ci is indicated by the blue cross north of the galaxy center.

nucleus along the minor axis), and from the halos of several edge-on galaxies. Many of them were known for star-forming or nuclear activity. Several of these galaxies have been or will be observed by XMM-Newton to constrain proposed equilibrium and non equilibrium models with better spectra and specifically to investigate if the X-ray spectra really point at strong subsolar metallicity in these plasma.

We have analyzed PV observations on NGC 253 and GT observations on NGC 253, NGC 2146, and NGC 3079. Unfortunately, the EPIC PN thin filter observations on these galaxies were hampered by strong background flaring. Here I will present a first EPIC PN colour image of NGC 3079 and then give more details on NGC 253.

NGC 3079 was observed by XMM-Newton in April 2001. The EPIC PN colour image (see Fig. 6) shows besides point sources in the field, sources within the optical D_{25} diameter of the galaxy that coincide with the ROSAT detected sources (Pietsch et al. 1998). The nuclear area is very bright and shows a hard spectrum. The hard source coincides with the radio nucleus whereas the softer bright nuclear emission is slightly offset to the E and originates from the nuclear outflow in this direction. The extended

diffuse emission from the outer disk and halo of NGC 3079 is mainly detected below 1 keV (red) and shows the morphology known from the ROSAT PSPC images. We do not see any source at the position of SN 2001ci, a type Ic supernova that exploded in NGC 3079 just four to twelve days after the XMM-Newton observation.

The PV observation of NGC 253 in July 2000 were split for EPIC PN in a 39 ks and a 14 ks exposure with medium and thin filter, respectively. While the first exposure mainly showed low background, half of the thin filter exposure had to be rejected due to background flaring. For a first analysis of the PV results see Pietsch et al. (2001). Our 24.5 ks GT observation of NGC 253 in December 2000 was pointed slightly offset from the nucleus into the NW halo. EPIC PN was used with the thin filter during the observation. Here we present some first results from this observation just for EPIC PN. Only 8.3 ks of the observation could be collected with low background while for the rest of the time the background was higher by a factor of at least two or even flaring.

Figure 7 allows us to compare EPIC images of the inner region of NGC 253 from the PV and GT observation. The images are colour coded according to the X-ray intensities in different bands with hard band contours superimposed. The EPIC data clearly reveal more point sources than the deep ROSAT observations (squares on PV image give sources from Vogler & Pietsch (1999)) and allow the mapping of diffuse emission in the disk. The underlying surface brightness at an energy of ~ 1 keV increases by factors of ~ 10 between disk, plume and extended nucleus.

All bright persistent sources known from the ROSAT observations are also detected by XMM-Newton. Some of the sources show brightness variations by factors of several compared to the ROSAT luminosities. In addition we detect at least 3 transient sources. The ROSAT source X12 was already classified as a transient by Vogler & Pietsch (1999) as it was only detected in the ROSAT observations in June 1992. X12 was again detected in the July 2000 XMM-Newton observations, however was not present in December 2000. Therefore, X12 has to be classified as a recurrent transient. A second bright transient was detected $\sim 70''$ SSW of the NGC 253 nucleus in the July 2000 observation and already was visible during the Chandra observation half a year earlier (Strickland et al. 2000). It was neither detected by ROSAT nor in the XMM-Newton GT observation in December 2000. A third transient is detected for the first time in the December 2000 XMM-Newton GT observation $\sim 45''$ NW of X23.

The brightest point source, X33 just south of the nucleus, varies by a factor of two during the PV observation and most likely is a black hole XRB as its spectrum can be modeled by an absorbed disk blackbody plus power law (see Fig. 9). Therefore the source is most likely a black hole XRB.

Einstein and ROSAT observations have revealed four diffuse X-ray emission components in NGC 253: the nu-

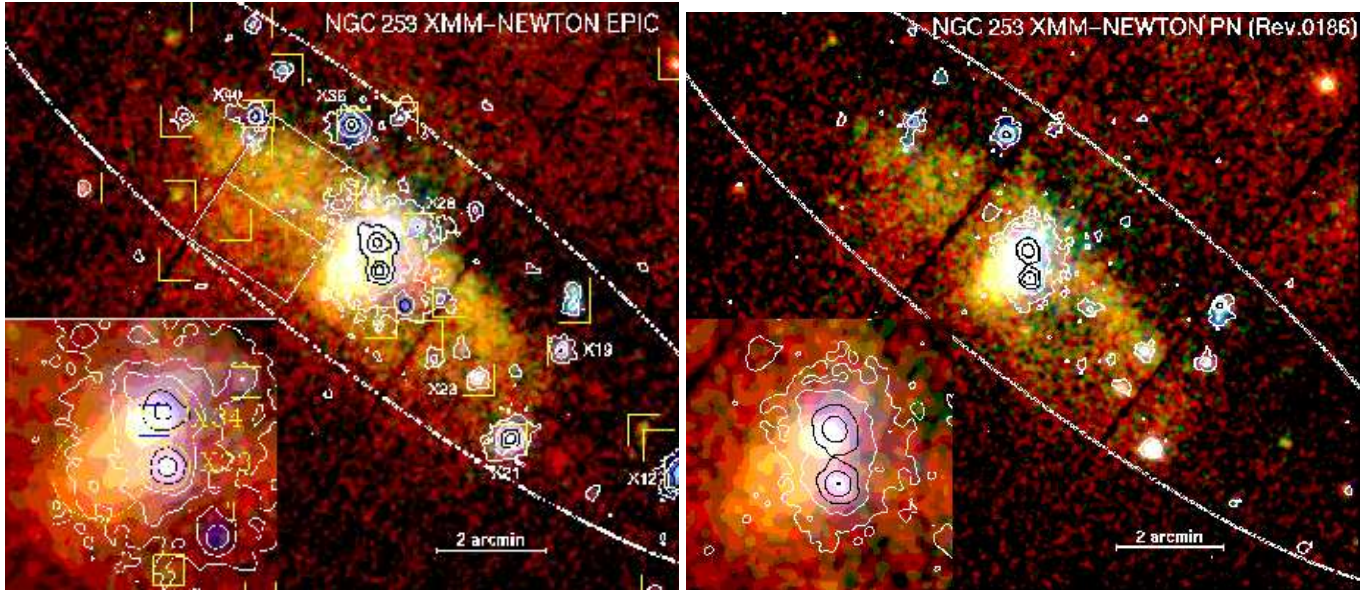


Figure 7. XMM-Newton EPIC low background images of the NGC 253. The colours represent X-ray intensities in different energy bands (red: 0.2–0.5 keV, green: 0.5–0.9 keV, blue: 0.9–2.0 keV), while the 2–10 keV emission is shown superimposed as contours. The white ellipse indicates the optical D_{25} diameter of the galaxy: (Left) PV observation from July 2000 (see Pietsch et al. 2001), combining all EPIC instruments. ROSAT sources from Vogler & Pietsch (1999) are indicated by squares. Spectral extraction regions are indicated. (Right) SSC GT observation from December 2000, using only EPIC PN

clear area, the plume, the galaxy disk, and especially the halo out to projected distances of 9 kpc from the disk (Fabiano & Trinchieri 1984, Fabiano 1988, and e.g. Pietsch et al. 2000b). The component with the softest spectrum originated from the halo of NGC 253, which was fitted in the ROSAT PSPC observations with a temperature of ~ 0.15 keV. While the slightly harder emission from the NW halo was already detected with *Einstein*, the soft response and the low background performance of the ROSAT PSPC was needed to detect the softer emission from the SE halo. It was therefore a challenge for the soft energy response of XMM-Newton if this halo emission could be detected.

The first three components are easily visible in the colour images (Fig. 7) and have been spectrally analyzed in some detail (see description of the PV results below). To search for the halo component, all EPIC PN low background thin filter observations were combined and the halo emission can be clearly detected in the 0.2–0.5 keV image. The spatial shape reflects that known from the ROSAT observations (Fig. 8). A detailed spectral analysis of the very extended halo component is in progress.

The EPIC images reveal unresolved emission from the inner disk that is harder along the inner spiral arms. EPIC PN spectra extracted NE of the nucleus, selecting areas of harder emission close to the major axis (N) and softer emission adjacent to the S (Fig. 8). While the spectra below 0.5 keV are very similar (Fig. 9), the NE(N) shows additional emission extending to energies of ~ 2 keV.

They both indicate emission lines from O VII and Fe XVII pointing at major hot plasma origin. The spectra have therefore been modeled assuming ISM components of solar abundance with two temperatures, shining through the ISM, i.e. correcting for the Galactic foreground and adding additional absorption within NGC 253. For the NE(N) spectrum a power law component had to be added which may describe contributions from unresolved point sources. The derived lower and higher temperatures (0.13 keV and 0.5 keV) agree in both areas within the errors, and the cooler component does not need additional absorption within NGC 253, indicating that the emission originates from the halo above the disk. These temperatures, derived over small areas, agree with the ROSAT results for the entire disk.

The nuclear region of NGC 253 is bright enough for a detailed study with both RGS and EPIC. The RGS spectrum (Fig. 10) is dominated by emission lines of hydrogenic and heliumlike charge states of the abundant low Z elements (N, O, Ne, Mg, Si) and the neonlike and fluorinelike charge states of Fe. With the help of EPIC, one can further localize the RGS emission components in the nuclear area. The strength of the Fe L lines relative to the K-shell lines suggests that collisional ionization is the dominant soft X-ray emission mechanism. The inferred temperatures range from 0.3 to 1.5 keV and the weakness of the longer wavelength lines suggests significant absorption. The general appearance of the RGS spectrum is reminiscent of the spectrum of intermediate age SNR gas, as

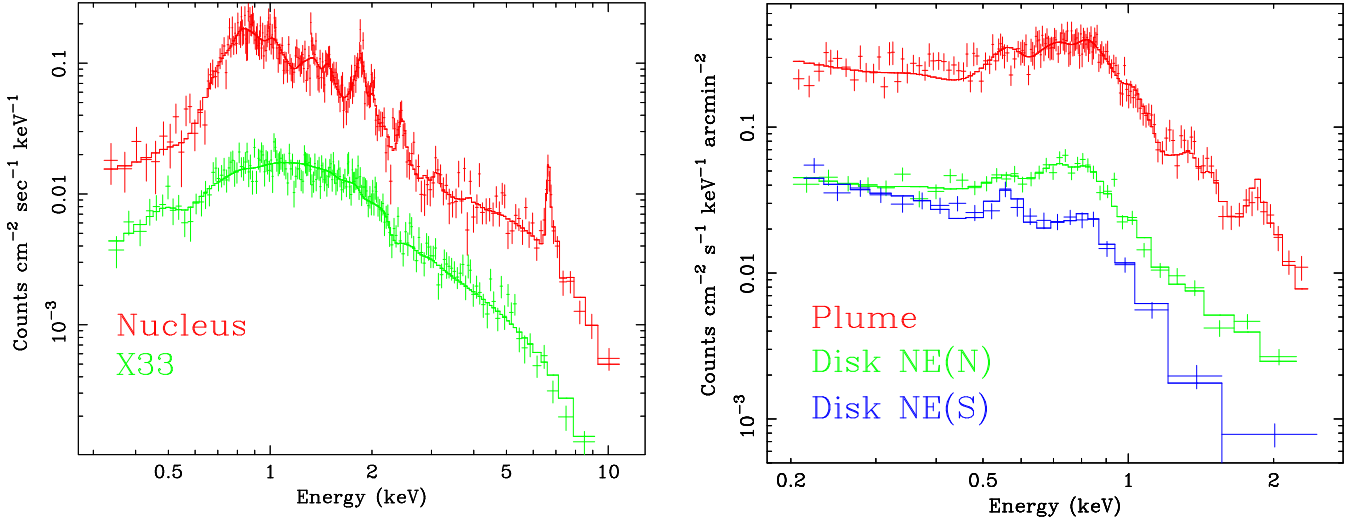


Figure 9. EPIC PN background subtracted spectra with spectral models indicated: **(Left)** spectra of the extended nucleus of NGC 253 and the XRB NGC 253-X33. **(Right)** spectra of the NGC 253 SE X-ray plume and two areas of the disk NE of the nucleus

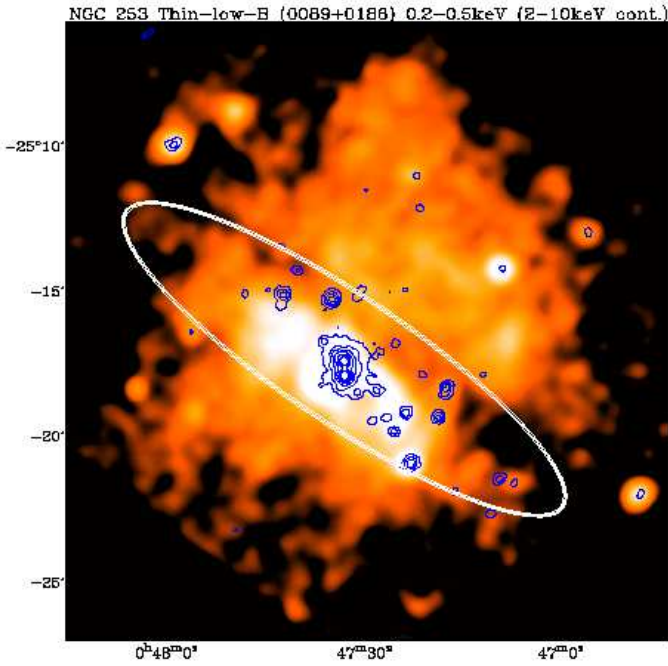


Figure 8. Smoothed EPIC PN thin filter low background 0.2-0.5 keV image of the NGC 253 field combining PV and SSC GT exposures. 2-10 keV emission is shown superimposed as blue contours. The white ellipse indicates the optical D_{25} diameter of the galaxy.

might be expected for a starburst nucleus and the interaction of the outflowing wind with the cooler gas of the ISM in the plume. In contrast to RGS, the EPIC instruments can spatially resolve the nuclear region in emission components from the unresolved nuclear source (X34) and the plume.

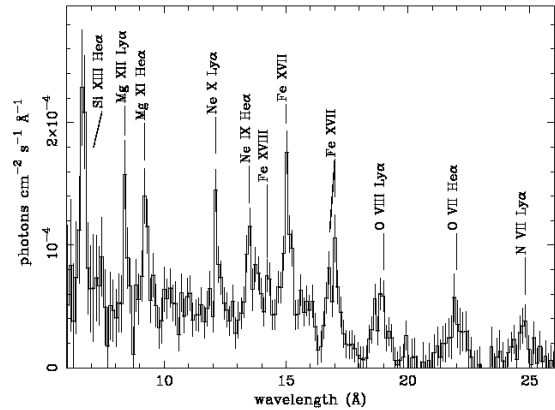


Figure 10. RGS spectrum of the bright nuclear area of NGC 253 covering nucleus and plume. Bright emission lines are identified.

No significant emission from X34 can be seen below 0.5 keV. As we go to higher energies, the centroid of the X34 emission shifts towards the position of the radio nucleus indicating that only at energies above 4 keV emission from the nuclear starburst will dominate the X-ray spectrum. The spectrum can be modeled using thin thermal plasma components of solar abundance with corresponding absorption increasing with the temperature of the plasma component, and an added power law component with the lowest absorption value. Three temperature components give an acceptable fit with $N_{\text{H}} = (0.34, 1.78, 13.2) \times 10^{22} \text{ cm}^{-2}$, photoindex of 1.0, and temperatures of (0.56, 0.92, 6.3) keV, respectively. A model with 0.7 solar abundance for all components and similar absorption and temperature values gives an equally acceptable fit and does

not need the power law component (Fig. 7). Note, that within the nuclear spectrum no evidence for a significant AGN contribution is detected (which would require a highly absorbed non-thermal component) and the very hard component can therefore be attributed purely to the starburst nucleus. Similar high-temperature plasma and Fe K lines have been found in young type Ib and type IIa SNRs. If one assumes that such SNRs are responsible for the X-ray emission of the starburst nucleus and that these SNRs would be strong iron line emitters for ~ 5000 yr, one can estimate that 1000 SNRs would be needed and the supernova rate of the NGC 253 starburst should be 0.2 yr^{-1} .

The EPIC images (Fig. 7) trace the bright X-ray plume emission of NGC 253 out to $1'75$ (1300 pc projected distance) from the nucleus along the minor axis of the galaxy disk to the SE into the galaxy halo, much further than possible with earlier observations. EPIC PN images for the different ionization state ions seen with the RGS reveal that the limb-brightening of the plume is mostly seen in higher ionization emission lines, while in the lower ionization lines, and below 0.5 keV, the plume is more homogeneously structured. The plume spectrum (Fig. 9) can be modeled by a three temperature thermal plasma containing the two low temperature nuclear components (though less absorbed) plus an unabsorbed 0.15 keV component similar to the disk spectra. These new findings point to new interpretations as to the make up of the starburst-driven outflow.

6. SUMMARY

The first observations of nearby late type galaxies have demonstrated the superb performance of the XMM-Newton instruments. However, sometimes high instrument background causes problems by strongly reducing the useful observation time below the times derived in the feasibility calculations and scheduled for observation. Another problem for homogeneous galaxy observations is imposed by the very stable XMM-Newton attitude control system which does not smear out small scale detector structures like CCD gaps or bad pixels. One therefore might argue for the introduction of a satellite dithering mode.

Besides these small obstacles, the big advantages of XMM-Newton for nearby galaxy studies compared to earlier observatories are the

- good spatial resolution and high collection power for EPIC and RGS spectra
- high detection potential for XRBs, X-ray pulsars, SNRs, CVs
- detectability of ISM and especially soft halo emission ($kT \approx 0.15$ keV) in low background EPIC PN thin filter observations
- advantage of simultaneous multi-instrument data collection

The first XMM-Newton observations promise a wealth of exciting results when new XMM-Newton nearby galaxy observations are performed and analyzed. The interpretation will certainly benefit when high spatial resolution *Chandra* observations of the galaxies are combined with the collecting power of XMM-Newton.

ACKNOWLEDGEMENTS

I thank my collaborators for their contributions to the work described above. The XMM-Newton project is an ESA Science Mission with instruments and contributions directly funded by ESA Member states and the USA (NASA). The XMM-Newton project is supported by the Bundesministerium für Bildung und Forschung / Deutsches Zentrum für Luft- und Raumfahrt (BMBF/DLR), the Max-Planck Society and the Heidenhain-Stiftung.

REFERENCES

- Behar, E., Rasmussen, A.P., Griffiths, R.G. et al. 2001, *A&A* 365, L242
- Dennerl, K., Haberl, F., Aschenbach, B. et al. 2001, *A&A* 365, L202
- Dubus, G., Charles, P.A., Long, K.S., Hakala, P.J., Kuulkers, E., 1999, *MNRAS* 302, 731
- Ehle, M., Pietsch, W., Haberl, F., 2001, in: *New Century of X-ray Astronomy*, eds. H. Inoue & H. Kunieda, ASP Conference Series 251, 300
- Fabbiano, G., 1988, *ApJ* 330, 672
- Fabbiano, G., Trinchieri, G., 1984, *ApJ* 286, 491
- Haberl, F., Pietsch, W., 1999, *A&AS* 139, 277
- Haberl, F., Filipović, M.D., Pietsch, W., Kahabka, P., 2000, *A&AS* 142, 41
- Haberl, F., Pietsch, W., 2001, *A&A* 373, 438
- Haberl, F., Dennerl, K., Filipović, M.D., Aschenbach, B., Pietsch, W., Trümper, J., 2001, *A&A* 365, L208
- Osborne, J.P., Borozdin, K.N., Trudolyubov, S.P. et al. 2001, *A&A* 378, 800
- Paerels, F., Rasmussen, A.P., Hartmann, H.W. et al. 2001, *A&A* 365, L303
- Pietsch, W., Trinchieri, G., Vogler, A., 1998, *A&A* 340, 351
- Pietsch, W., Vogler, A., Klein, U., Zinnecker, H., 2000a, *A&A* 360, 24
- Pietsch, W., Haberl, F., Ehle, M., Trinchieri, G., Vogler, A., 2000b, *AAS, HEAD meeting* 32, 21.04
- Pietsch, W., Roberts, T.P., Sako, M. et al. 2001, *A&A* 365, L174
- Rasmussen, A.P., Behar, E., Kahn, M.S., den Herder, J.W., van der Heyden, K., 2001, *A&A* 365, L231
- Sasaki, M., Haberl, F., Pietsch, W., 2000a, *A&AS* 143, 391
- Sasaki, M., Haberl, F., Pietsch, W., 2000b, *A&AS* 147, 75
- Sasaki, M., Stadlbauer, T.F.X., Haberl, F., Filipović, M.D., Bennie, P.J., 2001a, *A&A* 365, L237
- Sasaki, M., Haberl, F., Keller, S., Pietsch, W., 2001b, *A&A* 369, L29
- Shirey, R., Soria, R., Borozdin, K. et al. 2001, *A&A* 365, L195
- Soria, R., Wu, K., Page, M.J., Sakelliou, I., 2001, *A&A* 365, L273
- Strickland, D.K., Heckman, T.M., Weaver, K.A., Dahlem, M., 2000, *AJ* 120, 2965

- van der Heyden, K.J., Paerels, F., Cottam, J., Kaastra, J.S.,
Branduardi-Raymont, G., 2001, A&A 365, L254
- Vogler, A., Pietsch, W., 1999, A&A 342, 101
- Wu, K., Soria, R., Page, M.J., Sakelliou, I., Kahn, S.M., de
Vries, C.P., 2001, A&A 365, L267